

# Deformation in nanocrystalline metals

**It is now possible to synthesize polycrystalline metals made up of grains that average less than 100 nm in size. Such nanocrystalline metals contain a significant volume fraction of interfacial regions separated by nearly perfect crystals. The small sizes involved limit the conventional operation of dislocation sources and thus a fundamental question arises: how do these materials deform plastically? We review the current views on deformation mechanisms in nanocrystalline, face-centered cubic metals based on insights gained by atomistic computer simulations. These insights are discussed with reference to recent striking experimental observations that can be compared with predictions made by the simulations.**

Helena Van Swygenhoven<sup>1\*</sup> and Julia R. Weertman<sup>2</sup>

<sup>1</sup>*Condensed Matter Research with Neutrons and Muons, Paul Scherrer Institute, CH-5232 Villigen, Switzerland*

<sup>2</sup>*Department of Materials Science and Engineering, Northwestern University, Evanston, IL 60208, USA*

\*E-mail: [helena.vanswygenhoven@psi.ch](mailto:helena.vanswygenhoven@psi.ch)

Nanocrystalline metals are by definition polycrystalline structures with a mean grain size below 100 nm. Fig. 1 shows an image taken in a transmission electron microscope of a high-density nanocrystalline (nc)-Cu sample with a mean grain size of 20 nm. The mechanical behavior of a fully-dense nanocrystalline metal is, compared with its coarse-grain counterpart, characterized by a significantly enhanced yield stress and a limited tensile elongation<sup>1,2</sup>.

A simple extrapolation of conventional dislocation behavior to the nanometer regime might lead to the conclusion that plastic deformation is impossible at these small grain sizes and limited ductility is an intrinsic property of such material. Indeed, it is well known that the operation of the usual dislocation sources is grain-size

dependent<sup>3</sup>, in the sense that there is a critical length scale below which sources can no longer operate because the stress to bow out a dislocation approaches the theoretical shear strength. In face-centered cubic (fcc) metals, the critical grain size is believed to lie between 20–40 nm, depending on the nature of the dislocations being considered<sup>4</sup>. Further, the limited space offered by the nanocrystalline grains strongly limits the operation of the usual intragranular multiplication mechanisms<sup>5,6</sup>. So long as plasticity is predominantly the result of dislocation activity, the increase in strength with decreasing grain size can be explained on the basis of dislocation pile-ups at grain boundaries. This leads directly to the Hall-Petch relationship where the yield stress is proportional to the inverse square root of the average grain size<sup>1,7,8</sup>. As grain refinement continues, dislocation activity

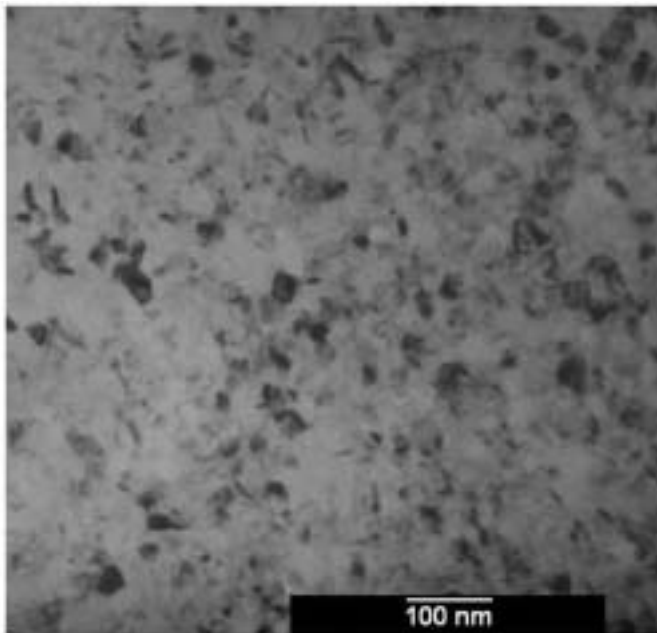


Fig. 1 Transmission electron micrograph of a 20 nm nc-Cu sample synthesized by inert gas condensation. (Courtesy of K. Zhang, Northwestern University.)

eventually becomes very difficult. However, with the increasing volume fraction of interfaces, grain boundary (GB) processes might become more effective and sometimes the material becomes softer with a further decrease in grain size, a situation known as inverse Hall-Petch behavior<sup>9</sup>. Fig. 2 shows a Hall-Petch plot for nc-Cu. The yield stress values were obtained from tensile, compression, and hardness tests on samples made by inert gas condensation<sup>10,11</sup>, cryogenic/room-temperature ball milling<sup>12,13</sup>, and surface material attrition treatment<sup>14</sup>. It can be seen that the points lie reasonably well on one curve whose initial slope has the same value as that of the Hall-Petch plot for coarse-grained Cu. The curve seems to begin bending over at the smallest grain sizes.

If dislocation plasticity is absent or impaired, the possibility of GB accommodation mechanisms involving GB sliding and/or Coble creep can be considered<sup>15</sup>. Strain rates associated with these processes are proportional to the GB diffusivity coefficient divided by a higher power of the grain diameter. Hence, deformation by these mechanisms is observed in polycrystalline material only at elevated temperatures. The possibility of higher effective GB diffusion coefficients in nanocrystalline metals, in addition to the large proportion of atoms affected by GBs (5-10% of atoms in a 20 nm grain-size sample) raises the hope that such diffusion-based mechanisms could become active at room temperature. However, experimental data on diffusion coefficients in nanocrystalline metals are very contradictory<sup>16</sup>.

### Looking for help in atomistic simulations

Massive parallel computing platforms offer the possibility of simulating multimillion atom samples using a molecular dynamics

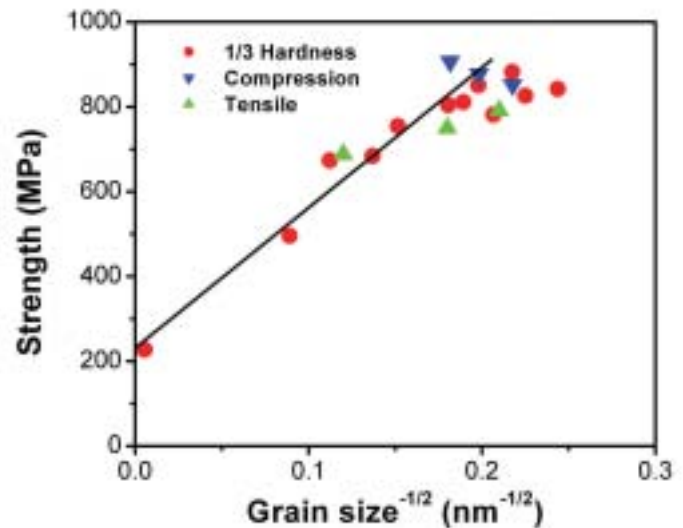


Fig. 2 Hall-Petch plot (yield strength versus inverse square root of the average grain size) for Cu. Yield strengths obtained from tension, compression, and hardness tests on nc-Cu synthesized by various methods are shown.

(MD) scheme and empirical potentials<sup>17</sup>. It is now possible to simulate three-dimensional nanocrystalline structures with, for instance, 15 grains of 30 nm diameter or 100 grains of 15 nm diameter; in other words, grain sizes of the same order as can be achieved experimentally<sup>18</sup>. The samples are usually built using a Voronoi procedure in which individual grains are geometrically constructed followed by an MD relaxation at room temperature<sup>19</sup>. Other procedures for the synthesis of three-dimensional samples are used, but they require more computing time<sup>20-22</sup>. When a special replica technique known as periodic boundary conditions is used, the sample can be considered a small part of an infinite bulk nanocrystalline metal. In order to reduce the number of atoms in a simulation, samples with a two-dimensional columnar GB network have been constructed in which the periodic boundary conditions are applied on ten atomic planes in the columnar direction<sup>23,24</sup>. In these samples, the GBs are perpendicular to the tensile directions and contain only twist-free misorientations, introducing additional simulation artifacts<sup>25</sup>. Fig. 3 shows a fully three-dimensional computational sample of an nc-Ni with a mean grain size of 10 nm. The color code is based on local crystallinity<sup>26</sup>: gray for atoms with an fcc neighborhood, red for atoms within a hexagonally close-packed (hcp) neighborhood, green for non-12-coordinated atoms, and blue for other 12-coordinated atoms. MD offers several other ways to characterize GB structures<sup>25</sup> using the centrosymmetry parameter<sup>27</sup>, positional disorder<sup>28</sup>, atomic potential energy, local hydrostatic pressure, or maximum resolved shear stress<sup>29,30</sup>. Figs. 4a and 4b show a GB taken out of an nc-Ni sample visualized by local crystallinity and hydrostatic pressure, respectively, demonstrating the different patterns obtained from the different criteria.

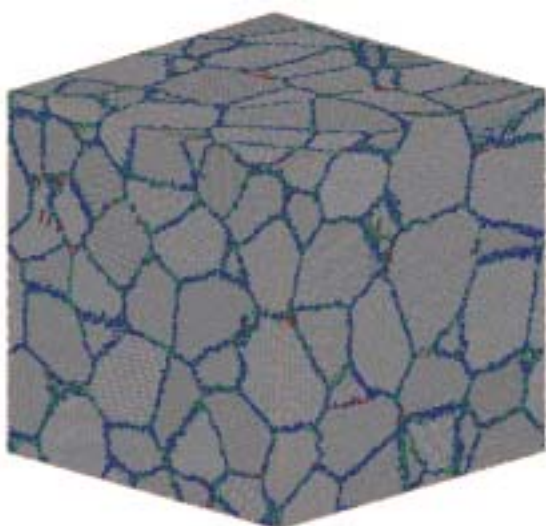


Fig. 3 Computational nc-Ni with a mean grain size of 10 nm using local crystallinity as color code: gray – fcc; red – hcp; green – non-12-coordinated; and blue – other 12-coordinated. (Reprinted with permission from<sup>18</sup>. © 2002 American Association for the Advancement of Science.)

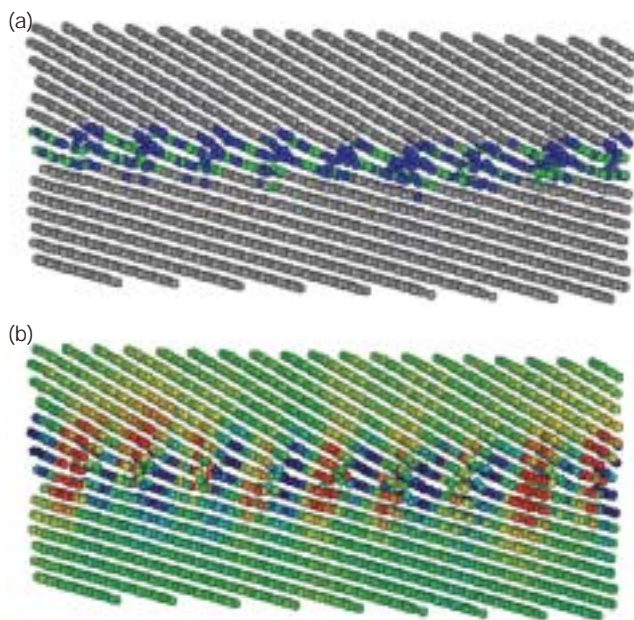


Fig. 4 Section of a GB with a 28° misorientation visualized with (a) local crystallinity color code, and (b) hydrostatic pressure (red = 2 GPa compression, blue = 2 GPa tension).

### Deformation behavior

Three-dimensional MD computer-generated samples have been used to study deformation behavior with the aim of comparing the results with experimental stress-strain data. For example, the stress-strain curves for a series of computer-generated Cu samples with average grain size ranging from 4.7 nm to 46.8 nm were calculated (Fig. 5a)<sup>31</sup>. The strain rate used in the simulations was  $5 \times 10^8/s$ , hence each of the curves represents a deformation time of 200 ps. The flow stress, taken to be

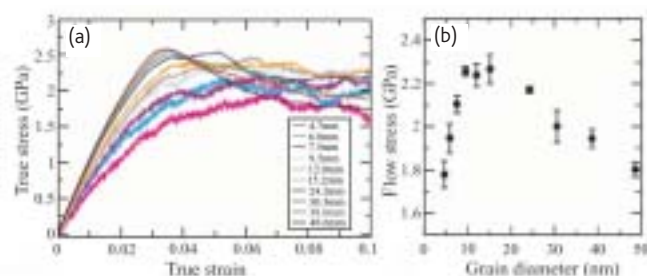


Fig. 5 (a) Stress-strain behavior for ten computational Cu samples with different grain sizes. (b) Grain size dependence of flow stress for the various samples. (Reproduced with permission from<sup>31</sup>. © 2003 American Association for the Advancement of Science.)

the more-or-less constant stress occurring after 6% strain, is plotted in Fig. 5b. A pronounced maximum is seen between grain sizes of 10 nm and 15 nm. The high values of the flow stress compared with experimental results, and its initial overshoot, were believed to be a consequence of the high strain rates used in the simulations<sup>31,32</sup>. Below the maximum flow stress, dislocation activity drops off. There is no detailed analysis of deformation mechanisms other than dislocation activity. It is questionable whether such 'macroscopic' stress-strain curves calculated by MD simulations can be compared with their experimental counterparts because of the high strain rates and short deformation times involved. Such high strain rates do not allow diffusion effects to occur, and hence structural accommodation in the GB is very limited<sup>25</sup>.

To investigate the possibility of Coble creep at room temperature, strain-time behavior has been simulated at very high temperatures, i.e. 0.7–0.9 of the melting temperature associated with the empirical potential, from which extrapolations toward room temperature were made<sup>33</sup>. Strain rates are calculated from the first 100 ps simulation time, as shown in Fig. 6. Dynamic equilibrium was assumed, a

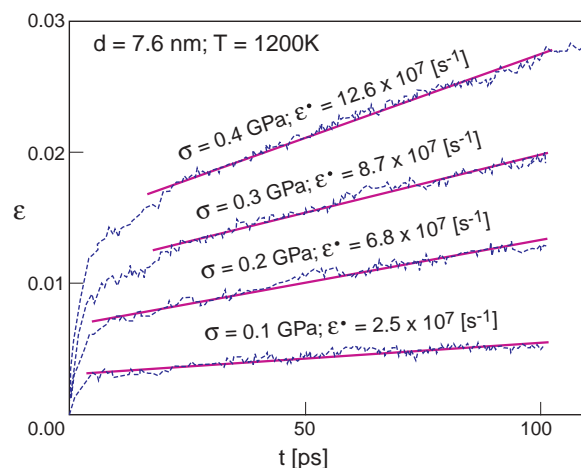


Fig. 6 Strain-time behavior for computational nc-Pd deformed at 0.85 of the melting temperature. The strain rates calculated from these curves are indicated. (Reproduced with permission from<sup>24</sup>. © 2002 Elsevier.)

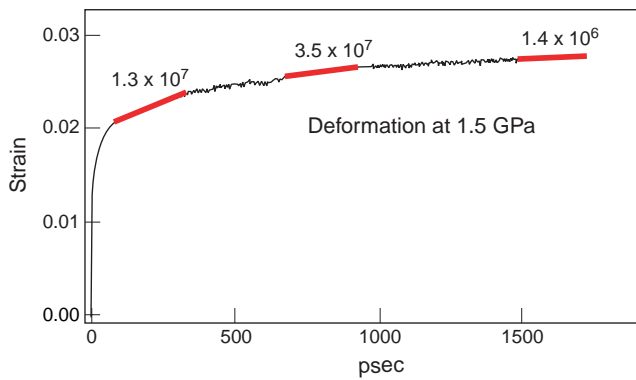


Fig. 7 Reduction in strain rate during deformation at constant uniaxial stress for a nc-Ni sample with mean grain size of 5 nm.

fundamental requirement for the application of a constitutive relation. It has been demonstrated, however, that at the nanosecond time scale, simulation strain rates of  $10^7/s$  steadily reduce by an order of magnitude (Fig. 7) over the first 1.5 ns, demonstrating that the activation energies and strain rates are calculated from a nonequilibrium state<sup>25</sup>.

### Deformation mechanism

It is therefore our view that the only meaningful information that can be extracted from simulations comes from a careful classification of the atomic processes taking place during deformation, and checking for changes in the behavior of these processes at the longest time scale possible, currently around a nanosecond. Although the same short time simulations are used as in the work described above, such an approach concentrates more on revealing the relations between GB structure and deformation mechanisms. However, here too the results can be prone to the presence of artifacts. Careful analysis of computer-generated samples subjected to deformation demonstrates both the possibility of GB sliding<sup>34</sup> and intragranular slip<sup>35,36</sup>, in which the GBs act as sources and sinks for dislocations. Both the inter- and intragrain processes are intimately linked to GB and triple junction (TJ) migration, and this can result in the formation of mesoscopic shear planes along which grains can slide collectively<sup>37</sup>, providing a possible explanation for the dimensions of the dimple structures seen in experimental fracture surfaces<sup>38</sup>.

In all simulated samples, GB sliding is observed as part of the observed plasticity. Careful analysis of the GB structure during sliding under constant tensile load shows that sliding includes a significant amount of discrete atomic activity (Fig. 8), either through uncorrelated shuffling of individual atoms or, in some cases, through shuffling involving several atoms acting with a degree of correlation<sup>34</sup>. In all cases the excess free volume present in the disordered regions plays an important role. In addition to the shuffling, hopping sequences involving several GB atoms have been observed. This type of atomic activity may be regarded as stress-assisted free volume migration. The

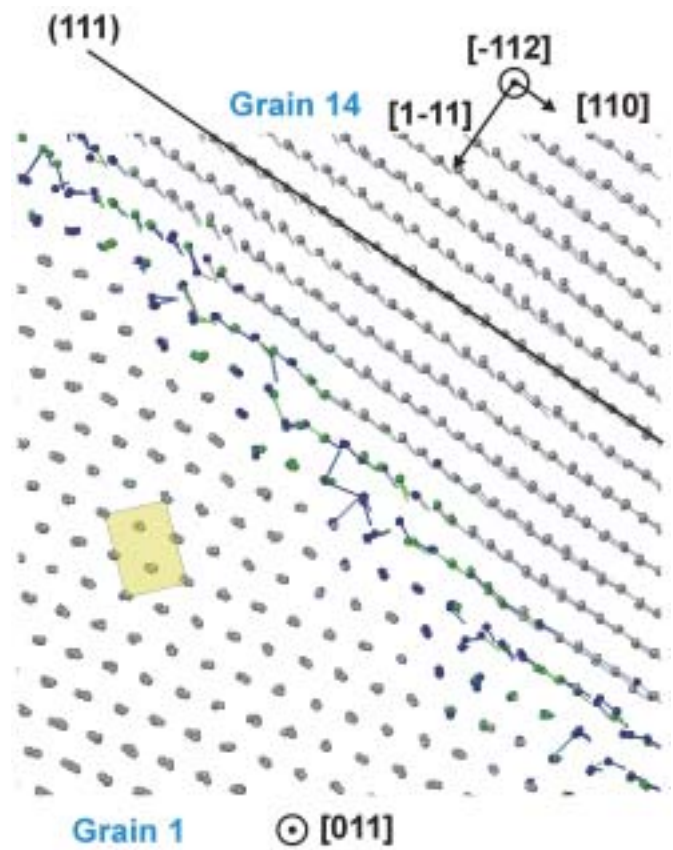


Fig. 8 Section of a GB showing sliding of the upper grain relative to the lower grain accompanied by atomic shuffles across the GB (displacement vectors indicate the change in position of the atoms, while a unit cell is shown in yellow). (Reproduced with permission from<sup>34</sup>. © 2001 American Physical Society.)

relative importance of GB sliding versus a dislocation mechanism is difficult to evaluate. It is reported that, after 10% deformation for nc-Cu with 5 nm grain size, dislocations account for only 3% of the strain<sup>32</sup>. However, these estimates pertain only to the extremely brief initial time period covered by the simulations. The percentage of strain covered by dislocation activity is likely to rise as the straining proceeds. On the other hand, it is worth noting that deformation in an Al sample with an average grain size of 5 nm takes place primarily by GB accommodation processes under a stress of 1.2 GPa. But raising the stress to 1.5 GPa switches the predominant deformation mechanism to the activity of full dislocations (our unpublished work). With this increase in stress, the strain rate changes from  $5 \times 10^7/s$  to  $10^9/s$ . However, both values are so unrealistic compared with experimental conditions that it is difficult to claim that in a 5 nm grain-size sample one mechanism gives way to the other.

The dislocation activity revealed by MD is called 'partial mediated' because single partial dislocations are emitted one at a time from the GBs (Fig. 9), a process often accompanied by stress-assisted free volume migration. Dislocations are usually emitted at GB ledges, but

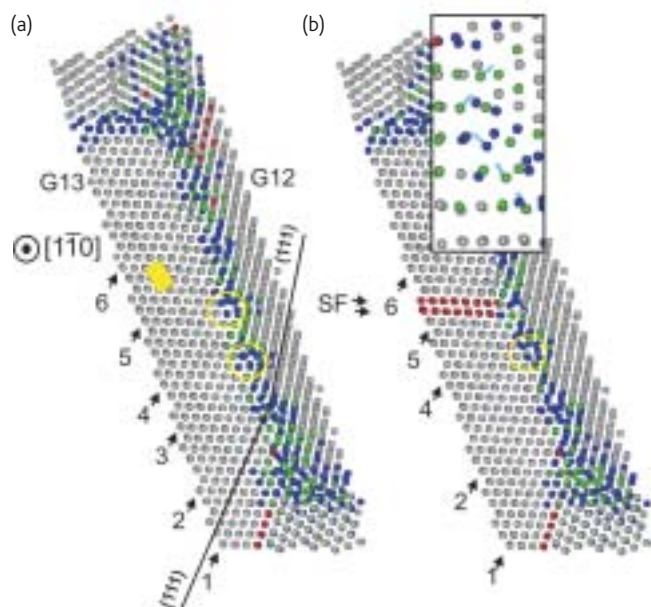


Fig. 9 Emission of a partial dislocation from a 12 nm sized GB: (a) configuration at elastic load, and (b) at 2.3% plastic strain. The stacking fault behind the partial is represented by the red hcp atoms. The inset shows the stress-assisted free volume migration. (Reproduced with permission from<sup>74</sup>. © 2003 Wiley-VCH.)

intersections of grown-in twin planes with general, high-angle GBs also seem to be very effective dislocation sources<sup>39</sup>. Whether there is only one partial emitted that travels across the grain and leaves behind a stacking fault (observed in simulations for Ni and Cu), or whether a trailing partial follows, leading to the formation of a full dislocation or

eventually a twin (observed in Al simulations), is a question that has been under heavy discussion. In an attempt to explain the different possibilities, several models have been proposed based on the absolute value of the stable stacking fault energy (SFE) and/or a critical grain size for the emission of a trailing dislocation based on the splitting distance<sup>40-42</sup>. Such an approach, while intuitively attractive, cannot explain all the simulation results since extended stacking faults are primarily observed for the material with the highest absolute value of the SFE. Moreover, the splitting distance cannot be used as a nucleation criterion since it assumes the existence of both partials. The nature of this slip activity can now be understood by considering the relative Peierls-type energy barriers for all possible partial dislocation-mediated processes represented in generalized planar fault (GPF) energy curves<sup>43</sup>. Given that the leading partial has already been nucleated, only full dislocations are observed in simulations for those materials for which the empirical potential has a ratio between the stable and unstable SFE of close to unity (Fig. 10). When twin structures are already present in the nanocrystalline grains, a similar approach using the GPF curves explains how plasticity is affected by twin migration<sup>44-46</sup>. How these simulations relate to experimental reality is still an open question, but it cannot be ruled out that the observation of extended stacking faults in Ni and Cu is an artifact of the MD simulation time scale and that, in all cases, the nucleation of both the leading and trailing partial dislocations would be seen if enough time were available. It should not be forgotten that the absence of impurities in the simulated GBs might enhance stress relief upon nucleation of the leading partial and therefore delay nucleation of the trailing dislocation. Such a scenario would be a straight-forward

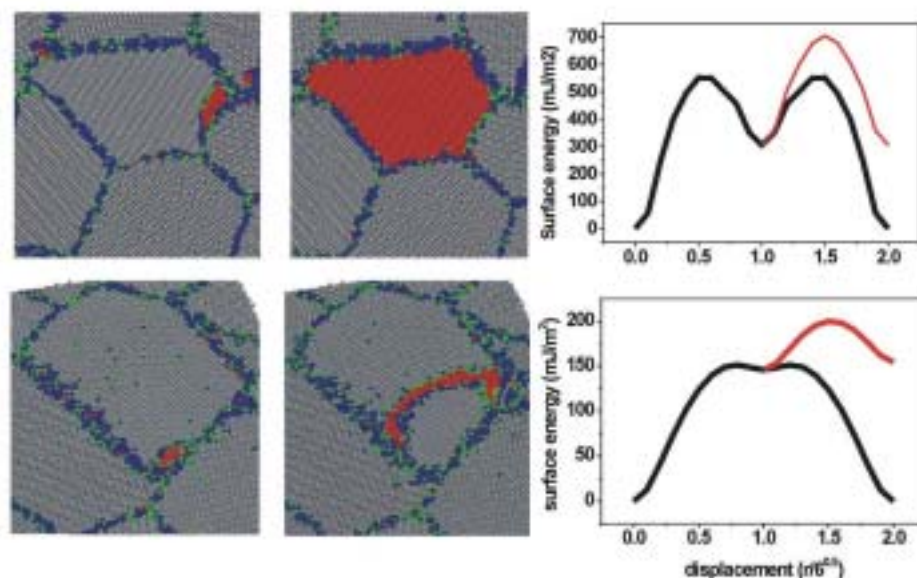


Fig. 10 Typical deformation mechanism observed in simulations of nc-Ni (two upper left-hand plots) and nc-Al (two lower left-hand plots). An extended partial is observed for nc-Ni, a full dislocation for nc-Al. The plots on the right-hand side show the general planar fault energy curves for the two potentials used (black: formation of a partial-full dislocation, red: formation of a twin). (Reproduced with permission from<sup>43</sup>. © 2004 Nature Publishing Group.)

interpretation since there is no experimental evidence of the buildup of a dense network of stacking faults after tensile deformation in nc-Ni and nc-Cu. *Post mortem* transmission electron microscopy (TEM) analysis has demonstrated the sporadic existence of large stacking faults, but not as a dominant bulk mechanism. *In situ* TEM straining studies<sup>41,47,48</sup> report “sudden contrast changes” during deformation, which were interpreted to be the result of dislocation activity. No development of stacking faults was observed. *In situ* X-ray diffraction (XRD) studies of nc-Ni during tensile loading and unloading revealed the reversibility of diffraction peak broadening, demonstrating the lack of a permanent residual dislocation network<sup>49,50</sup>. These observations support the idea that predominantly full dislocations are emitted and subsequently absorbed or reabsorbed in the GBs, leaving no footprint behind.

The suggestions from MD, together with the experimentally observed increase in strength<sup>1,11</sup>, the low values of the measured activation volume ( $10-20b^3$ , where  $b$  is the Burgers vector)<sup>12,51,52</sup>, and the ten-times higher strain rate sensitivity<sup>51,52</sup> in nanocrystalline metals, have inspired the development of several analytical models. For instance, dislocation sources in GBs have been described as Frank-Read sources where the length of the source is proportional to the grain size<sup>53,54</sup>. A different approach has been recently suggested by Asaro and Suresh<sup>55</sup> in which dislocations are pictured as emitted from stress concentrations at the GBs. This approach is similar to that of Rice<sup>56</sup> for dislocation emission from a crack tip. The picture that is envisaged is a sliding GB facet at which a stress concentration is built up. The length of the mode II crack is taken as the length of the facet, introducing in this way a grain-size dependency. Asaro and Suresh explicitly specify that the sliding envisioned does not constitute gross GB sliding, and therefore does not contribute to finite deformation nor to the limits of the material's strength. After the thermally activated dislocation nucleation process, the resulting dislocation loop reaches a critical size at which point it expands athermally and henceforth is completely mechanically driven. From this critical size, they obtain an activation volume of  $\sim 3-10b^3$ . An important ingredient of the model is that the dislocation propagation within the grain is not hindered by the GB, and therefore the model precludes the possibility that after dislocation nucleation the GB might also constitute an important rate-limiting process in dislocation-mediated nanocrystalline plasticity. This picture however is not supported by *in situ* XRD measurements<sup>57</sup> performed at 180 K, which show a nonreversible peak broadening at low temperatures that can be recovered after warming the sample to 300 K. These measurements provide evidence for a thermally activated pinning-depinning mechanism, indicating that not only nucleation but also propagation has a thermal component, a picture also suggested by recent temperature-dependent activation volume measurements<sup>51</sup>.

There are, however, a number of details of dislocation nucleation/propagation/absorption revealed by MD simulations that do not support the picture of a simple operating Frank-Read source located in

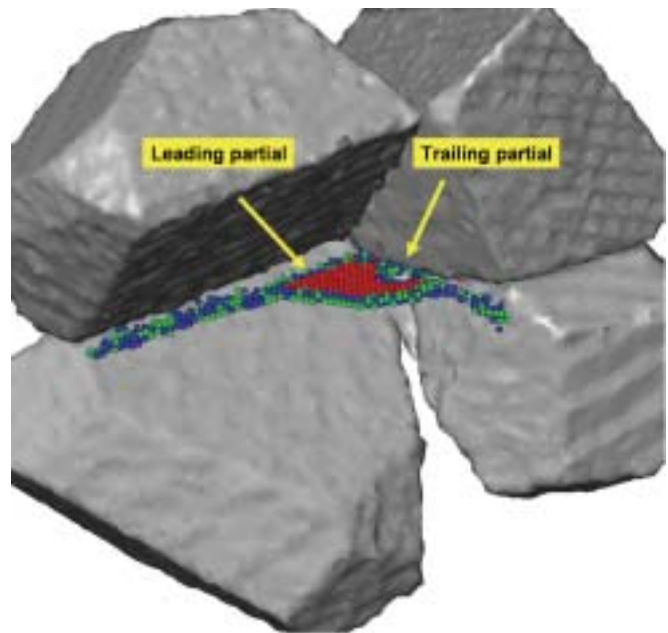


Fig. 11 Full dislocation in an nc-Al sample. Leading and trailing partials have been nucleated at different grain boundaries. (Reproduced with permission from<sup>58</sup>. © 2006 Elsevier.)

the GBs<sup>58</sup>. For instance, a dislocation source in a GB seems to operate only once. Upon nucleation taking place, accompanied by stress relief and atomic shuffles, the GB ledge is removed. Leading and trailing partials are usually nucleated at different areas, even sometimes at different GBs, solely determined by the GBs themselves (Fig. 11). The only length scale that could be assigned to a source would be the distance between the ledges, however that length is largely determined by the GB structure and to a lesser extent by the grain size. Furthermore, partials are often observed to nucleate but not propagate, remaining as extrinsic GB dislocation segments. Once a full dislocation is traveling, the propagation depends on the structure of the adjacent GBs. Temporary pinning at ledges results in enlarged splitting distances (Fig. 12) and unpinning is strongly temperature dependent, suggesting that nucleation and propagation are separate processes. Upon depinning, debris of the dislocation line may be deposited on a GB. However, time restrictions of the simulations do not allow an investigation to see if such debris can act as a new dislocation source<sup>58</sup>.

Local GB migration and changes in the configurations of the TJs are observed to accompany dislocation nucleation/propagation and absorption. Fig. 13 shows the local migration of a noncoherent twin boundary taken out of nc-Al (a) before and (b) after the nc-Al had been involved in the emission and absorption of several dislocations<sup>39</sup>. Whether the GB migration observed in MD simulations can be related to the recent observations of grain coarsening during deformation is an open question. It has been shown for nc-Cu that grains coarsen under the stress field of an indenter, and that the coarsening occurs even

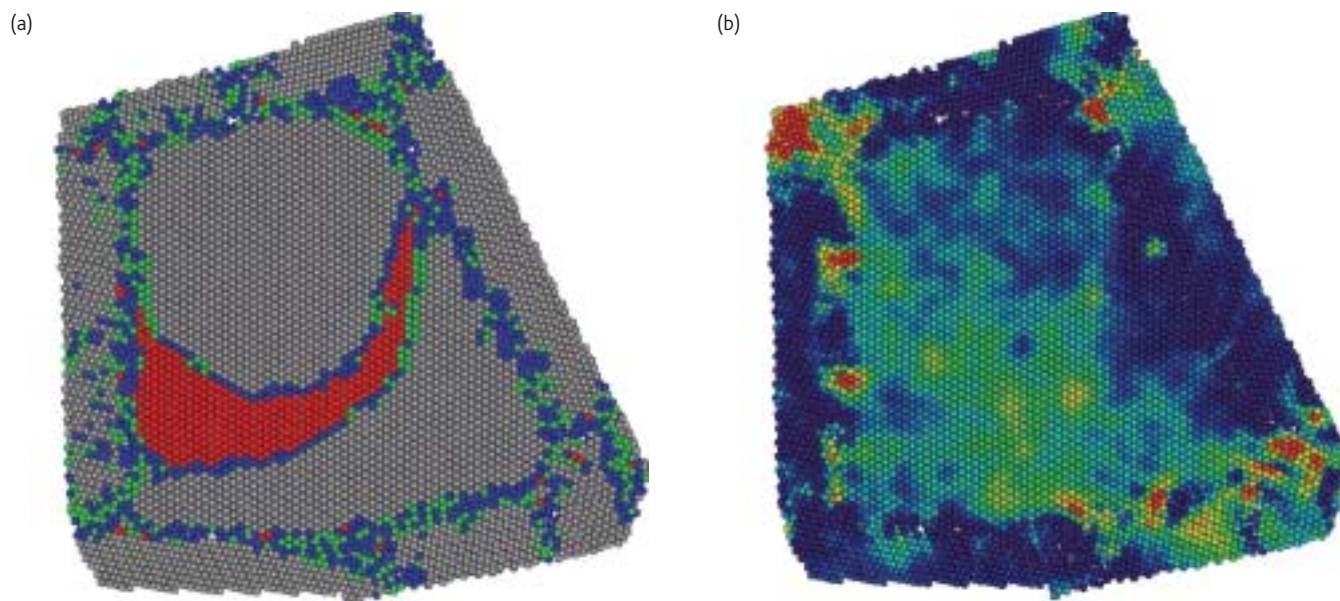


Fig. 12 A full dislocation traveling through an nc-Al grain visualized with (a) local crystallinity and (b) hydrostatic pressure. The dislocation is pinned for a while at the left-hand side GB, where stress fluctuations are present. No pinning is observed in the right-hand side GB that is under uniform tension.

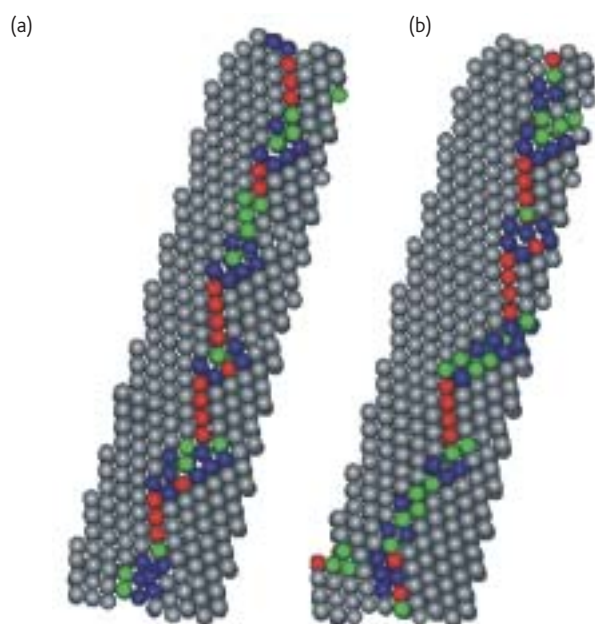


Fig. 13 View of a noncoherent twin boundary in an nc-Al sample (a) before and (b) after the GB was involved in the emission and absorption of several dislocations. (Reproduced with permission from<sup>39</sup>. © 2006 Elsevier.)

when the indentation is performed at liquid nitrogen temperatures<sup>11,59</sup>. Similarly, it has been shown that extensive plasticity can be obtained in a free-standing, submicrometer-thick nc-Al film only when grain coarsening is involved<sup>60</sup>. Unless very high temperatures are applied, the time limitations inherent to the MD technique do not allow the study of coarsening in realistic three-dimensional simulations<sup>61</sup>. The limited

tensile ductility in actual nanocrystalline metals has made the comparison of pre- and post-deformed samples for signs of coarsening and GB migration difficult. The influence of other aspects related to grain coarsening, such as impurities, the special stress patterns associated with indentation or those that occur in a free-standing film, or the presence of special boundaries have, as yet, to be investigated.

### Future directions

Most simulations have been performed on pure samples containing general, high-angle GBs with a narrow grain size distribution, the grains being defect-free. Preliminary studies have shown the importance of low-angle GBs and other types of special boundaries incorporated into a nanocrystalline GB network<sup>62,63</sup>, as well as the effect of impurities on coarsening<sup>64,65</sup>. All of these are microstructural features that may be found in experimental samples. Their study will benefit from simulations and experiments performed in bicrystals to investigate the mechanical behavior of single interfaces<sup>66-71</sup>, thus allowing identification of particularly interesting GBs. For instance, the coupling between the normal motion and the shear strain in any flat tilt GB can result in GB migration that does not involve diffusion or sliding<sup>70,71</sup>. Detailed studies on the effect of curvature are an extremely important additional aspect in the determination of migration mechanism<sup>72,73</sup>. It is of interest to investigate how the incorporation of such GBs could influence the stability of the nanocrystalline GB network.

There is no doubt that atomistic simulations have provided unprecedented insight into the structural and mechanical properties of nanocrystalline materials. However, the extrapolation of this

knowledge to the experimental regime requires a clear understanding of the temporal and spatial scales of the modeling technique and a detailed structural characterization of the simulated samples. The high stress/ short time restrictions inherent to the method make it impossible to determine the true rate-limiting processes. Therefore, atomistic simulations alone are not suited, at present, for setting up a deformation map for nanocrystalline metals analogous to that used in

constitutive plasticity, where the suggested mechanisms are quantified in terms of applied stress, grain size, strain rates, and temperature.

The ultimate goal, however, is that atomistic simulations will reveal to us the necessary conditions that a GB and a GB network must fulfill in order to allow the operation of an efficient deformation mechanism, thus providing a working scheme for experimentalists. [mt](#)

## REFERENCES

- Weertman, J. R., In: *Nanostructured materials; processing, properties and applications*, Koch, C. C., (ed.), William Andrews Publishing, Norwich, NY, (2002), 397
- Kumar, K. S., et al., *Acta Mater.* (2003) **51**, 5743
- Arzt, E., *Acta Mater.* (1998) **46**, 5611
- Legros, M., et al., *Philos. Mag. A* (2000) **80**, 1017
- Kocks, U. F., Mecking H., *Prog. Mater. Sci.* (2003) **48**, 171
- Gilman, J. J., *Appl. Micromech. Flow Solids* (1953), 185
- Hall, E. O., *Proc. R. Soc. London, Ser. B* (1951) **64**, 474
- Petch, N. J., *J. Iron Steel Inst.* (1953) **174**, 25
- Masumura, R. A., et al., *Acta Mater.* (1998) **46**, 4527
- Sanders, P. G., et al., *Mater. Sci. Eng. A* (1997) **234-236**, 77
- Zhang, K., et al., *Appl. Phys. Lett.* (2004) **85**, 5197
- Cheng, S., et al., *Acta Mater.* (2005) **53**, 1521
- Youssef, K. M., et al., *Appl. Phys. Lett.* (2005) **87**, 91904
- Wang, Y. M., et al., *Scripta Mater.* (2003) **48**, 1581
- Li, Y. J., et al., *Mater. Sci. Eng. A* (2004) **387-389**, 585
- Schaefer, H.-E., et al., *Mater. Sci. Eng. A* (2000) **286**, 24
- Heermann, D. W., *Computer Simulation Methods*, Springer-Verlag, (1986)
- Van Swygenhoven, H., *Science* (2002) **296**, 66
- Van Swygenhoven, H., et al., *Phys. Rev. B* (2000) **62**, 831
- Hou, M., et al., *Phys. Rev. B* (2002) **66**, 195408
- Zhang, Y. W., et al., *Acta Mater.* (2004) **52**, 5105
- Kebllinski, P., et al., *Scripta Mater.* (1999) **41**, 631
- Yamakov, V., et al., *Nat. Mater.* (2002) **1**, 45
- Yamakov, V., et al., *Acta Mater.* (2002) **50**, 61
- Derlet, P. M., et al., *Scripta Mater.* (2003) **49**, 629
- Honeycutt, D. J., and Andersen, H. C., *J. Phys. Chem.* (1987) **91**, 4950
- Kelchner, C. L., et al., *Phys. Rev. B* (1998) **58**, 11085
- Derlet, P. M., and Van Swygenhoven, H., *Phys. Rev. B* (2003) **67**, 014202
- Cormier, J., et al., *J. Appl. Phys.* (2001) **89**, 99
- Samaras, M., et al., *Phys. Rev. B* (2003) **68**, 224111
- Schiøtz, J., and Jacobsen, K. W., *Science* (2003) **301**, 1357
- Schiøtz, J., et al., *Phys. Rev. B* (1999) **60**, 11971
- Wolf, D., et al., *Acta Mater.* (2005) **53**, 1
- Van Swygenhoven, H., and Derlet, P. M., *Phys. Rev. B* (2001) **64**, 224105
- Van Swygenhoven, H., et al., *Phys. Rev. B* (2002) **66**, 024101
- Derlet, P. M., et al., *Philos. Mag. A* (2003) **83**, 3569
- Hasnaoui, A., et al., *Phys. Rev. B* (2002) **66**, 184112
- Hasnaoui, A., et al., *Science* (2003) **300**, 1550
- Frøseth, A. G., et al., *Scripta Mater.* (2006) **54**, 477
- Yamakov, V., et al., *Nat. Mater.* (2004) **3**, 43
- Liao, X. Z., et al., *Appl. Phys. Lett.* (2004) **84**, 3564
- Shimokawa, T., et al., *Modell. Simul. Mater. Sci. Eng.* (2005) **13**, 1217
- Van Swygenhoven, H., et al., *Nat. Mater.* (2004) **3**, 399
- Frøseth, A. G., et al., *Acta Mater.* (2004) **52**, 5863
- Frøseth, A. G., et al., *Appl. Phys. Lett.* (2004) **85**, 5863
- Frøseth, A. G., et al., *Adv. Eng. Mater.* (2005) **7**, 16
- Hugo, R. C., et al., *Acta Mater.* (2003) **51**, 1937
- Kumar, K. S., et al., *Acta Mater.* (2003) **51**, 387
- Budrovic, Z., et al., *Science* (2004) **304**, 273
- Budrovic, Z., et al., *Appl. Phys. Lett.* (2005) **86**, 231910
- Wang, Y. M., and Ma, E., *Appl. Phys. Lett.* (2004) **85**, 2750
- Dalla Torre, F., et al., *Acta Mater.* (2002) **50**, 3957
- Cheng, S., et al., *Acta Mater.* (2003) **51**, 4505
- Chen, M., et al., *Science* (2003) **300**, 1275
- Asaro, R. J., and Suresh, S., *Acta Mater.* (2005) **53**, 3369
- Rice, J. R., *J. Mech. Phys. Solids* (1992) **40**, 239
- Brandstetter, S., et al., *Appl. Phys. Lett.* (2005) **85**, 231910
- Van Swygenhoven, H., et al., *Acta Mater.* (2006) **54**, 1975
- Zhang, K., et al., *Appl. Phys. Lett.* (2005) **87**, 61921
- Gianola, D. S., et al., *Acta Mater.* (2006), in press
- Haslam, A. J., et al., *Acta Mater.* (2004) **52**, 1971
- Frøseth, A. G., et al., *Acta Mater.* (2005) **53**, 4847
- Caturla, M.-J., et al., *Appl. Phys. Lett.* (2004) **84**, 598
- Millett, P. C., et al., *Acta Mater.* (2005) **53**, 3671
- Millett, P. C., et al., *Acta Mater.* (2006) **54**, 297
- Spearot, D. E., et al., *Acta Mater.* (2005) **53**, 3579
- Zhang, H., et al., *Acta Mater.* (2004) **52**, 2569
- Sansoz, F., and Molinari, J. F., *Acta Mater.* (2005) **53**, 1931
- Hoagland, R. G., et al., *Scripta Mater.* (2004) **50**, 775
- Cahn, J. W., et al., *Philos. Mag. A* (2006), in press
- Winning, M., and Rolett, A. D., *Acta Mater.* (2005) **53**, 2901
- Winning, M., *Scripta Mater.* (2006) **54**, 987
- Winning, M., et al., *Acta Mater.* (2002) **50**, 353
- Van Swygenhoven, H., et al., *Adv. Eng. Mater.* (2003) **5**, 345